

Cite this: DOI: 10.1039/c0xx00000x

www.rsc.org/xxxxxx

ARTICLE TYPE

Composite of Hierarchical Interpenetrating 3D Hollow Carbon Skeleton from Lotus Pollen and Hexagonal MnO₂ Nanosheets for High-Performance Supercapacitors

Electronic Supplementary Information

5

Hongpeng Li,^a Bin Wang,^a Xinyi He,^a Jun Xiao,^d Hongseng Zhang,^a Qi Liu,^a Jingyuan Liu,^a Jun Wang,^{* a,c} Lianhe Liu^c and Peng Wang^{* b}

^aKey Laboratory of Superlight Material and Surface Technology, Ministry of Education, College of Materials Science and Chemical Engineering, Harbin Engineering University, Harbin 150001, P. R. China. E-mail: zhqw1888@sohu.com; Fax: +86 451 8253 3026; Tel: +86 451 8253 3026

^bState Key Laboratory of Polymer Physics and Chemistry, Changchun Institute of Applied Chemistry, Chinese Academy of Sciences, Changchun 130022, P. R. China

^cInstitute of Advanced Marine Materials, Harbin Engineering University, Harbin 150001, P. R. China

^dCollege of Mechanical and Electrical Engineering, Harbin Engineering University, Harbin 150001, P. R. China

15 *Corresponding author.

1. Experiment Section

20 Pre-carbonation lotus pollen (PCLP)

The structure of the pollen grain roughly consists of two parts: a thick, hard, inflexible shell and a thin, tender, flexible inner core (consisting of pectin, amino acids, vitamins, proteins and other essentials). The shell comprises an inner wall and an outer wall. The inner and outer walls connect with many columellas (rods). The main components of the outer shell are sporopollenin, cellulose and hemicelluloses. In addition, the shell has a strong resistance to acid and alkali.¹ Initially, to remove surface impurities and all protoplasm in the core, a pre-carbonation process was carried out. Typically, 16.0 g natural lotus pollen grains were dispersed in 100 mL anhydrous ethanol with ultrasonication for 1 h. Then, the lotus pollen grains were filtered and washed with a large amount of distilled water. The filtrate was milky white, indicating that proteins and other impurities had dissolved in ethanol. The alcohol-treated lotus pollen grains were placed in an alcoholic solution of formaldehyde (volume ratio = 1:1), with magnetic stirring for 5 min and allowed to stand for 5 min for fixing the unique morphology of pollen grains. After that, pollen grains were suction filtered and washed with copious distilled water. Finally, the above pollen grains were added into 100 mL of 10 M H₂SO₄ solution with magnetic stirring in a water bath at 60 °C for 1 h. During this period, the water in sporopollenin and cellulose or hemicelluloses, was removed by sulfuric acid. The color of lotus pollen grains gradually changed from yellow to medium brown, which showed that the pollen grains had been carbonized. After that, the medium brown lotus pollen grains were suction filtered and washed to neutral with a large amount of distilled water, then dried for 12 h at 60 °C in an oven.

35 Preparation of hierarchical MnO₂/C composite

The MnO₂/C composite was prepared by means of a simple and rapid dipping process according to the following steps: 0.25 g medium brown PCLP grains were added into 50 mL of 0.5 M KMnO₄ aqueous solution and magnetically stirred for 10 min to ensure the pollen grains were dispersed. For comparing the effects of immersion time on the morphology and properties of the samples, different dipping times (1 h, 2 h, 3 h, 4 h and 5 h) were used to prepare MnO₂/pollen grains precursors. After standing for different periods at room temperature, the black product was washed with plenty of distilled water and suction filtered. Then the product (MnO₂/pollen grains precursors) was dried at 60 °C for 12 h.

To obtain the hierarchical interpenetrating 3D hollow MnO₂/C composite, MnO₂/pollen grains precursors were calcined in a tube furnace at 500 °C for 2 h with a heating rate of 5 °C/min under N₂ atmosphere. The carbon material treated at 500 °C contains many oxygen functional groups, which are benefit for enhancing the wettability and cycling stability of the carbonaceous materials. The resultant samples were named as MnO₂/C-t, where t was the dipping time; therefore, the above prepared samples were respectively addressed as MnO₂/C-1, MnO₂/C-2, MnO₂/C-3, MnO₂/C-4 and MnO₂/C-5.

5 Moreover, for comparison, carbonized lotus pollens (CLP) were also prepared under the above process except dipping in KMnO₄ aqueous solution.

MnO₂ nanoparticles

As a comparison, MnO₂ nanoparticles were synthesized via a simple method.² Briefly, 10 mL anhydrous ethanol and 10 mL 5 M KMnO₄ aqueous solution were mixed and soaked for 3 h at room temperature. The product was centrifuged and washed with distilled water and ethanol, then dried at 60 °C for 12 h.

10 2. Characterization

The crystalline structures of the obtained samples were determined by a powder X-ray diffraction system (XRD, Rigaku TTR-III) equipped with Cu K α radiation ($\lambda=0.15406$ nm). The X-ray photoelectron spectroscopy (XPS) measurements were performed by a Thermo ESCALAB 250Xi spectrometer with monochromated Al K α radiation ($h\nu=1486.6$ eV). All XPS spectra were calibrated with respect to the C1s peak at 284.6 eV. Fourier-transform infrared (FT-IR) spectra were collected with an AVATAR 360 FT-IR spectrophotometer using a standard KBr pellet technique. Thermal analysis (TGA) was carried out, ranging from room temperature to 700 °C in Ar at a heating rate of 10 °C/min using a NETZSCH STA 409 thermogravimetric analyzer. The morphology and microstructure of the as-prepared materials were investigated by using field-emission scanning electron microscopy (FESEM, Hitachi SU8000) and transmission electron microscopy (TEM, PHILIPS CM 200 FEG, 160 kV).

3. Electrochemical measurements

20 Electrochemical measurement was carried out on a CHI 660D electrochemistry workstation (Shanghai Chenhua Instrument, Inc.). The working electrode was made by mixing the active materials, acetylene black and PTFE (tetrafluoroethylene) with a weight ratio of 85 : 10 : 5, pasting on a piece of nickel foam (1×1 cm²), and dried under vacuum at 60 °C for 12 h. The weight of the active material was about 5 mg. Cyclic voltammetry (CV) measurements, galvanostatic charge/discharge and electrochemical impedance spectroscopy (EIS) were studied in a conventional three-electrode system equipped with a platinum electrode and a saturated calomel electrode (SCE) as 25 counter and reference electrodes, respectively. And the electrolyte was 1 M Na₂SO₄ aqueous solution. All the tests were carried out at room temperature.

The specific capacitance derived from the cyclic voltammetry (C, Eq.1) and charge-discharge (C_s, Eq.2) curves of the electrode are calculated from the following equations:

$$C = \frac{\int I(V)dV}{v \times m \times \Delta V} \quad (1)$$

30
$$C_s = \frac{I \times t}{m \times \Delta t} \quad (2)$$

where I is the instant current on the CV curves and the discharge current (A), v is potential scan rate (mV/s), m is the mass of the electroactive materials in the electrodes (g), V is the total potential deviation (V) and t is the time in seconds of the discharge, respectively.³

The Coulombic efficiency was calculated according to the Eq. 3:⁴

35
$$\eta = \frac{I_d}{I_c} \quad (3)$$

where t_c and t_d stand for the time of charge and discharge, respectively.

The energy density (E, Eq. 4) and power density (P, Eq. 5) are calculated from the following equations:⁵

$$E = \frac{1}{2} CV^2 \quad (4)$$

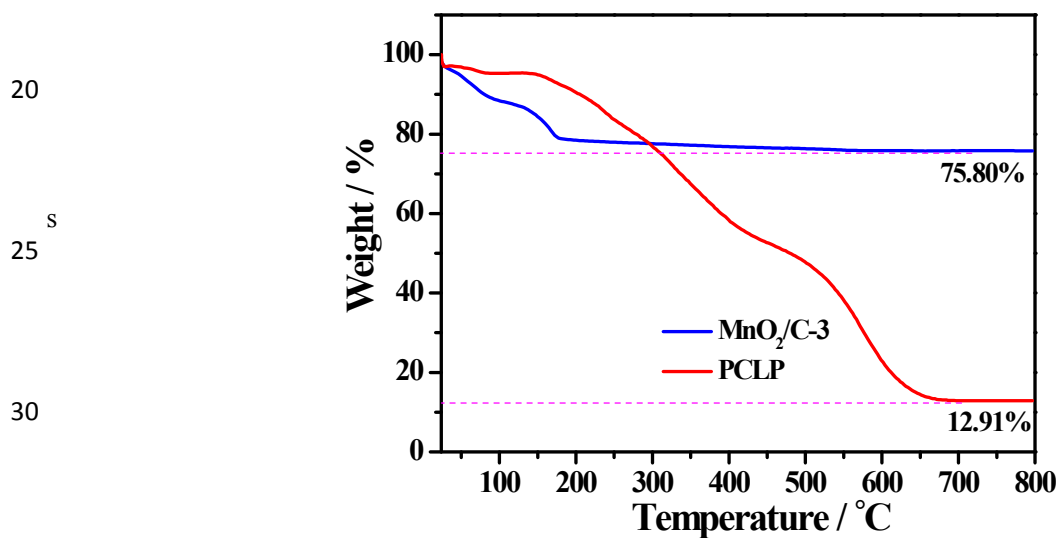
$$P = \frac{E}{t} \quad (5)$$

where E, C, V, P and t represent the energy density (Wh/kg), specific capacitance (F/g), operation potential (V), power density (W/kg) and the discharge time, respectively.

5

10

15 4. Thermal analysis of PCLP and MnO₂/C-3 composite recorded in O₂ atmosphere



35 Fig. S1 TGA curve of PCLP and MnO₂/C-3 composite recorded in O₂.

40

45

5. SEM images of MnO₂ nanoparticles and carbonized lotus pollens

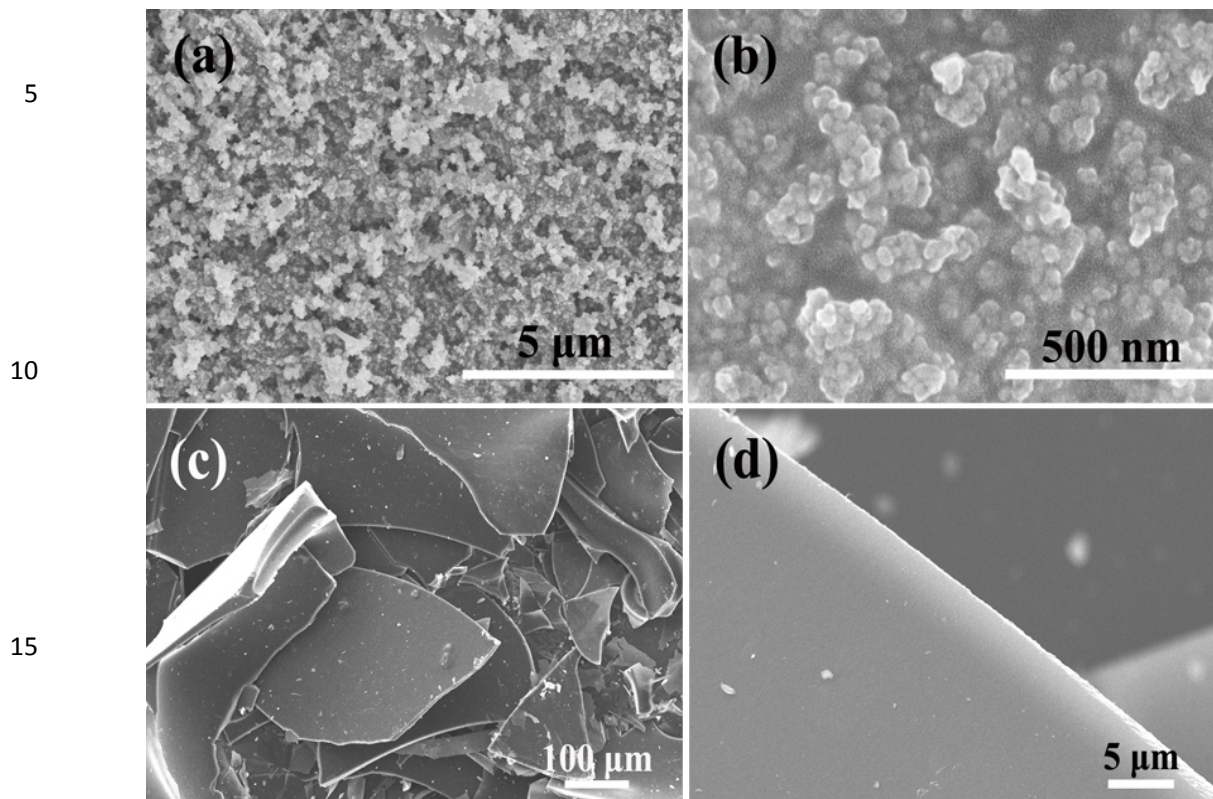


Fig. S2 SEM images of with different magnifications. (a, b) MnO₂ nanoparticles; (c, d) carbonized lotus pollens (CLP)

6. Nyquist plots for MnO₂/C-3 composite, pure MnO₂ and CLP

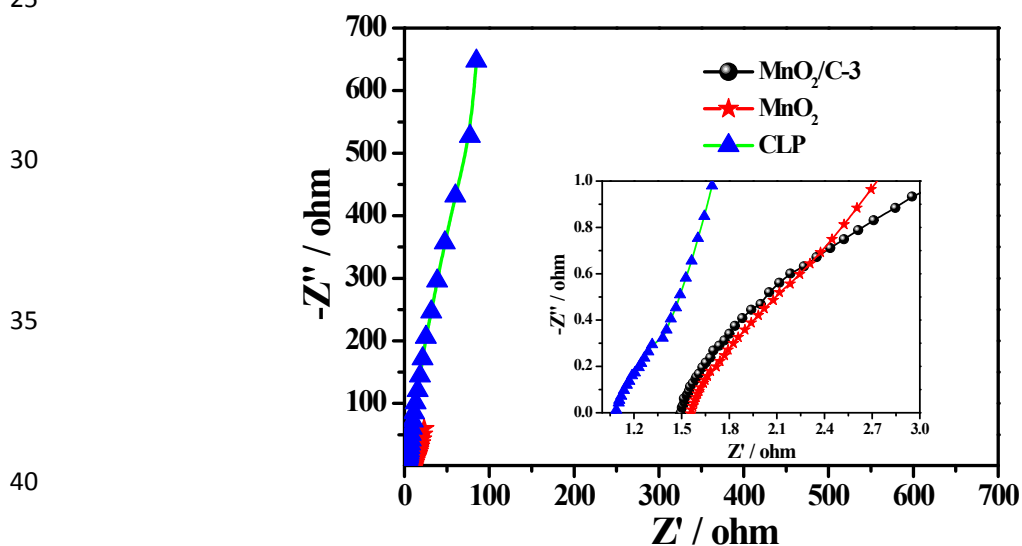
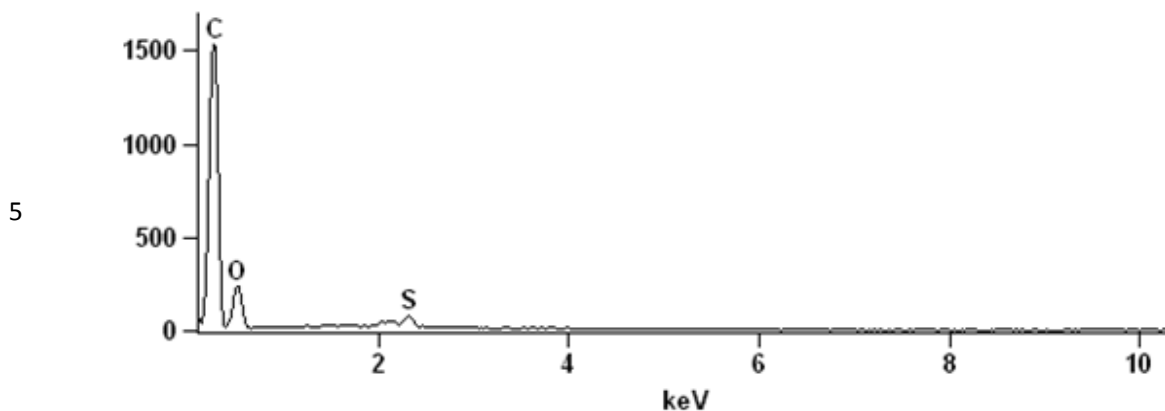


Fig. S3 A comparison of Nyquist plots for MnO₂/C-3 composite, pure MnO₂ and CLP.

7. EDS spectrum of the PCLP grains



10 Fig. S4 EDS spectrum of the PCLP grains

The chemical compositions for PCLP grains were characterized by EDS (see Fig. S4 and Table S1). The results show that the chemical compositions of the PCLPs consist of C, O and S. The abundant oxygen atoms on pollen surface participate in the Faraday reactions to enhance the pseudocapacitance properties and improve the wettability of carbon matrix. Moreover, a small amount of sulfur atoms is also helpful to improve the electrochemical properties of materials.³

8. SEM images of MnO₂/C-1, MnO₂/C-2, MnO₂/C-4, MnO₂/C-5

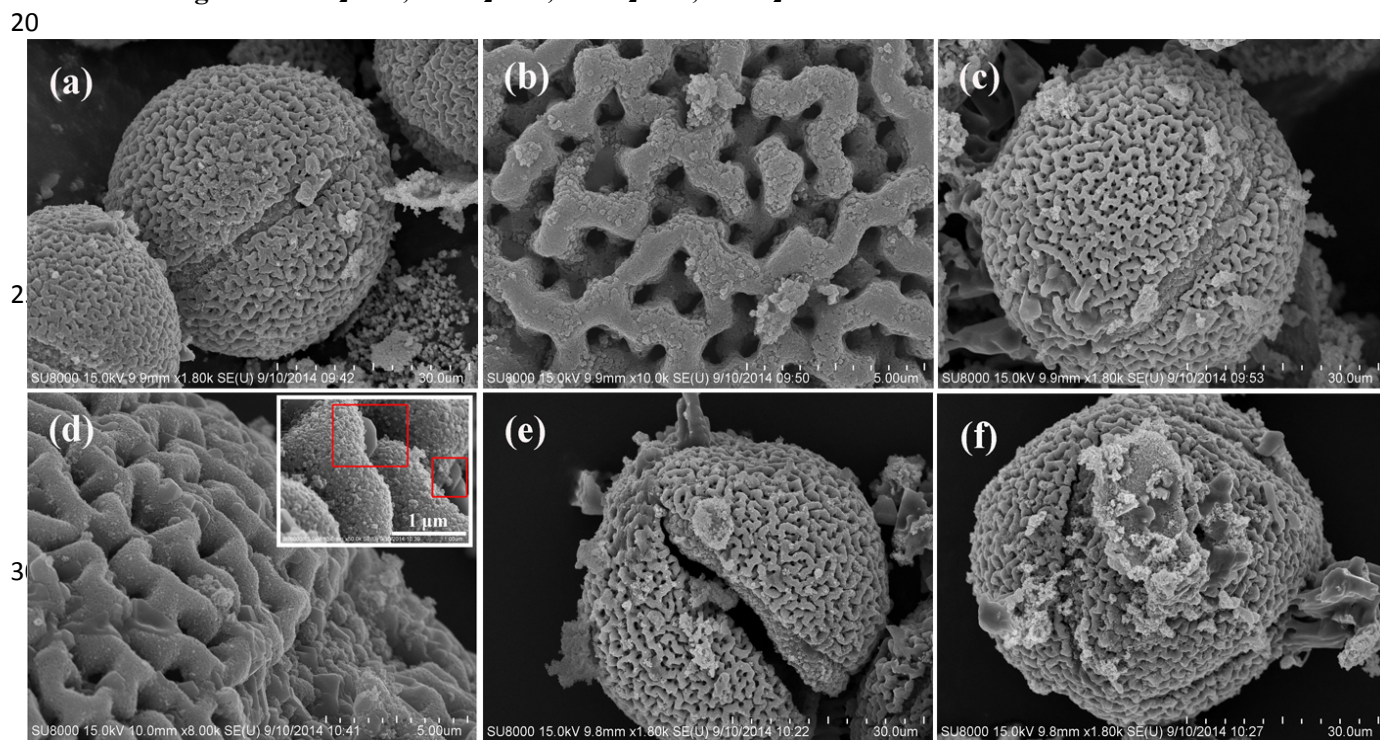


Fig. S5 Different magnification SEM images of (a) and (b) MnO₂/C-1 composite; (c) and (d) MnO₂/C-2 composite, inset is the enlarged image; (e) MnO₂/C-4 composite and (f) MnO₂/C-5 composite.

There are only a few MnO₂ nanoparticles coated onto the pre-carbonized pollen grain surfaces for the MnO₂/C-1 composite. Yet, the presence of manganese dioxide nanoparticles means the redox reaction did occur between KMnO₄ and pre-carbonized pollen grains. Then, after immersing in KMnO₄ solution for 2 hours, many nanoparticles form and the sizes become bigger (Fig. S5(c)). At the same time, small MnO₂ nanosheets appear among nanoparticles (Fig. S5(d)). With an extended immersion time, the hexagonal MnO₂ nanosheets successfully form as a result of further growth of nanoparticles. With the direct carbon-MnO₄⁻ reaction continuing, MnO₂ nanosheets in situ anchor onto the surfaces of pollen grains to form a unique structure as shown in Fig. 3. When the immersion time was increased to 4 and even 5 hours, the stable formation of pollen grains microspheres is destroyed by direct-contact reaction between pollen grains and the high concentration of KMnO₄ (see Fig. S5(e) and (f)).

10

9. CV and galvanostatic charge/discharge cures of MnO₂/C-1, MnO₂/C-2, MnO₂/C-4, MnO₂/C-5

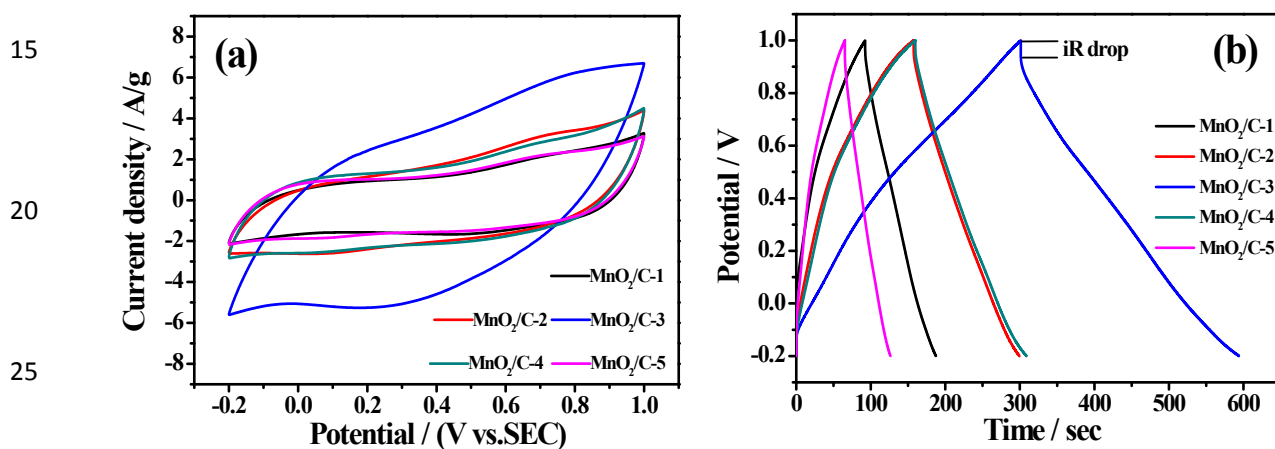


Fig. S6 A comparison of CV curves at 25 mV/s (a) and galvanostatic charge/discharge curves at a current density of 1 A/g (b) for 30 MnO₂/C-1, MnO₂/C-2, MnO₂/C-3, MnO₂/C-4 and MnO₂/C-5 composite.

All CV curves reveal a quasi rectangular shape, and, the area of the CV curve for the MnO₂/C-3 electrode is even larger than others,. Also, the galvanostatic charge/discharge curves of the MnO₂/C composites (Fig. S6(b)) are almost linear and symmetrical. As observed, the discharge time for MnO₂/C-3 is higher than others, which is in agreement with the quantity indicated by CV. From Fig. S6(b), we can obviously discover the discharge time for MnO₂/C-5 is the shortest. With the extension of the reaction time, a great deal of cellulose or hemicelluloses was consumed by KMnO₄, leading to the decrease of electrical conductivity and the damage. As a result, the electrochemical properties of MnO₂/C-5 are not as good as others.

40

45

10. CV and galvanostatic charge/discharge curves of MnO₂ and MnO₂/C-5

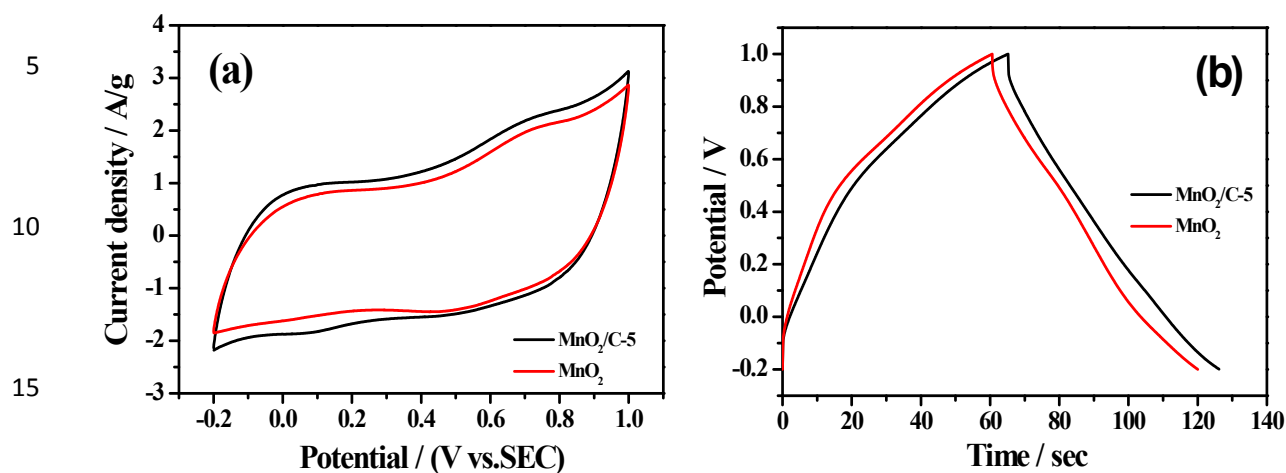


Fig. S7 The comparison of CV curves at 25 mV/s (a) and galvanostatic charge/discharge curves at a current density of 1 A/g (b) for pure 20 MnO₂ and MnO₂/C-5 composite.

Although the electrochemical properties of MnO₂/C-5 are not as good as MnO₂/C-1, MnO₂/C-2, MnO₂/C-3 and MnO₂/C-4, yet they are superior to pure MnO₂ nanoparticles. Fig. S7 has shown the comparison of CV curves at 25 mV/s and galvanostatic charge/discharge curves at a current density of 1 A/g for pure MnO₂ and MnO₂/C-5 composite. Obviously, the area of the CV curve for the MnO₂/C-5 electrode is larger than pure MnO₂ nanoparticles. And the discharge time is longer. Therefore, we can draw a conclusion: the carbon skeleton can enhance the conductivity and improve the overall electrochemical properties of as-prepared MnO₂/C composites.

30

11. EDS spectra of PCLP

element	Weight %			Atom %		
	C	O	S	C	O	S
percent	68.37	31.21	0.42	74.35	25.48	0.17

Table S1 Chemical composition of PCLP grains determined by EDS measurement.

35

40

45

12. Comparison of the specific capacitances of carbon-based electrodes.

Materials	Cs (F/g)	Electrolyte	Ref.
Hydrazine reduced graphene oxide	123 (10 mV/s)	6 M KOH	6
Ordered mesoporous carbon nanospheres	173 (1 mA/cm ²)	6 M KOH	7
Activated porous carbon	223 (1 mV/s)	6 M KOH	8
Activated carbon xerogel microspheres	251 (0.125 A/g)	1 M H ₂ SO ₄	9
Porous graphene nanosheets	241 (2 mV/s)	6 M KOH	10
High density porous graphene macroform	238 (0.1 A/g)	6 M KOH	11
Seaweeds derived carbon (ALG-C)	198 (2 mV/s)	1 M H ₂ SO ₄	12
Oil palm empty fruit bunch fibers (SACG)	135 (10 mA/cm ²)	1 M H ₂ SO ₄	13
Carbons derived by pyrolysis of coffee shells	156 (1 mV/s)	6 M KOH	14
Cherry stones-based activated carbons	230 (1 mA/cm ²)	2 M H ₂ SO ₄	15
Red cedarwood-based biochar	115 (0.5 A/g)	0.5 M H ₂ SO ₄	16
Nitrogen-doped carbon based on peptides of hair	134.5 (5 A/g)	6 M KOH	17
Carbons Derived from Fungi (P-HT-A)	196 (5 mV/s)	6 M KOH	18
Carbon Derived from Paulownia Sawdust	227 (2 mV/s)	6 M KOH	19
MnO ₂ -doped, polyaniline-grafted rice husk ash nanocomposites (PANI/MnO ₂ /RHA)	135 (0.5 mA/g)	0.5 M Na ₂ SO ₄	20
MnO ₂ loaded biomass carbonaceous aerogel composites (MnO ₂ @CA)	123.5 (5 mV/s)	6 M KOH	21
MnO₂/C-3 composite	257 (0.5 A/g)	1 M Na₂SO₄	This work

Table S2 Comparison of the specific capacitances of carbon and MnO₂ based electrodes.

5

References

- 1 Y. Wang, Z. M. Liu, B. X. Han, Y. Huang and G. Y. Yang, *Langmuir*, 2005, **21**, 10846.
- 2 H. Pang, S. M. Wang, G. H. Li, Y. H. Ma, J. Li, X. X. Li, L. Zhang, J. S. Zhang and H. H. Zheng, *J. Mater. Chem. A*, 2013, **1**, 5053.
- 3 G.Y. Zheng, L.B. Hu, H. Wu, X. Xie and Y. Cui. *Energy Environ. Sci.*, 2011, **4**, 3368.
- 10 4 A. Cuna, N. Tancredi, J. Bussi, V. Barranco, T. A. Centeno, A. Quevedo and J. M. Rojo, *J. Electrochem. Soc.*, 2014, **161**, A1806.
- 5 J. Yan, Q. Wang, T. Wei and Z. J. Fan, *Adv. Energy Mater.*, 2013, **4**, 1.
- 6 J. Yan, T. Wei, B. Shao, F. Ma, Z. J. Fan, M. L. Zhang, C. Zheng, Y. C. Shang, W. Z. Qian and F. Wei, *Carbon*, 2010, **4**, 1731.
- 7 X. L. Yu, J. G. Wang, Z. H. Huang, W. C. Shen and F. Y. Kang, *Electrochem. Commun.*, 2013, **36**, 66.
- 8 K. S. Xia, Q. M. Gao, J. H. Jiang and J. Hu, *Carbon*, 2008, **46**, 1718.
- 15 9 Z. Z. Benabithé, F. C. Marin, J. de Vicente and C. M. Castilla, *Langmuir*, 2013, **29**, 6166.
- 10 Z. J. Fan, Q. K. Zhao, T. Y. Li, J. Yan, Y. M. Ren, J. Feng and T. Wei, *Carbon*, 2012, **50**, 1699.
- 11 Y. Tao, X. Y. Xie, W. Lv, D. M. Tang, D. B. Kong, Z. H. Huang, H. Nishihara, T. Ishii, B. H. Li, D. Golberg, F. Y. Kang, T. Kyotani and Q. H. Yang, *Sci. Rep.*, 2013, **3**, 2975.
- 12 E. R. Piñero, F. Leroux and F. Béguin, *Adv. Mater.*, 2006, **18**, 1882.
- 20 13 B. N. M. Dolah, M. Deraman, M. A. R. Othman, R. Farma, E. Taer, Awitdrus, N. H. Basri, I. A. Talib, R. Omar and N. S. M. Nor, *Mater. Res. Bull.*, 2014, **60**, 10.
- 14 M. R. Jisha, Y. J. Hwang, J. S. Shin, K. S. Nahm, T. P. Kumar, K. Karthikey, N. Dhanikaivelu, D. Kalpana, N. G. Renganath and A. M. Stephan, *Mater. Chem. Phys.*, 2009, **115**, 33.
- 15 M. O. Marin, J. A. Fernández, M. J. Lázaro, C. F. González, A. M. García, V. G. Serrano, F. Stoeckli and T. A. Centeno, *Mater. Chem. Phys.*, 2009, **114**, 323.
- 25 16 J. H. Jiang, L. Zhang, X. Y. Wang, N. Holm, K. Rajagopalan, F. L. Chen and S. G. Ma, *Electrochim. Acta*, 2013, **113**, 481.
- 17 Z. H. Guo, Q. W. Zhou, Z. J. Wu, Z.G. Zhang, W. Zhang, Y. Zhang, L. J. Li, Z. Z. Cao, H. Wang and Y. F. Gao, *Electrochim. Acta*, 2013, **113**, 620.
- 18 H. Zhu, X. L. Wang, F. Yang and X. R. Yang, *Adv. Mater.*, 2011, **23**, 2745.
- 30 19 X. G. Liu, M. T. Zheng, Y. Xiao, Y. H. Yang, L. F. Yang, Y. L. Liu, B. F. Lei, H. W. Dong, H. R. Zhang and H. G. Fu, *ACS Appl. Mater. Interfaces*, 2013, **5**, 4667.

20 P. Prabunathan, K. Sethuraman and M. Alagar, *RSC Adv.*, 2014, **4**, 47726.

21 Y. M. Ren, Q. Xu, J. M. Zhang, H. X. Yang, B. Wang, D. Y. Yang, J. H. Hu and Z. M. Liu, *ACS Appl. Mater. Interfaces*, 2014, **6**, 9689.